A study of overcast, partly cloudy and clear skies by global illuminance and its variation features

Lou, Siwei; Li, Danny H W; Chen, Wenqiang

Published in:
IOP Conference Series: Materials Science and Engineering

Published: 01/01/2019

Document Version:
Final Published version, also known as Publisher's PDF, Publisher's Final version or Version of Record

Published version (DOI):
10.1088/1757-899X/556/1/012015

Publication details:
Lou, S., Li, D. H. W., & Chen, W. (2019). A study of overcast, partly cloudy and clear skies by global illuminance and its variation features. *IOP Conference Series: Materials Science and Engineering*, *556*, [012015]. https://doi.org/10.1088/1757-899X/556/1/012015

A study of overcast, partly cloudy and clear skies by global illuminance and its variation features

IOP Conf. Series: Materials Science and Engineering **556** (2019) 012015 doi:10.1088/1757-899X/556/1/012015

A study of overcast, partly cloudy and clear skies by global illuminance and its variation features

Siwei Lou[1,*], Danny H W Li[2] and Wenqiang Chen[2]
[1]School of Civil Engineering, Guangzhou University, 230 Guangzhou Higher Education Mega Centre West Outer Ring Road, Panyu District, Guangzhou, China
[2]Building Energy Research Group, Department of Architecture and Civil Engineering, City University of Hong Kong, Tat Chee Avenue, Kowloon, Hong Kong SAR, China
*E-mail: swlou2-c@my.cityu.edu.hk

Abstract. The diffuse radiance and luminance distribution in the skydome can determine the solar energy on the building envelope in various orientations and under complex obstructions. The diffuse sky is anisotropic for clear and partly cloudy skies, while isotropic for overcast skies. Thus, identifying the sky conditions are essential to the sky radiance and luminance studies. Previously developed approaches using statistic data suffered from data shortage and inaccuracy. Sunlight under cloudy skies may frequently be blocked, causing the high-frequency illuminance fluctuations. The illuminance should variate smoothly under clear skies without clouds. In this work, we studied the horizontal irradiance time series, its variation frequency, and its relationship to the sky conditions determined by the luminance scan. The work contributes to identifying the sky conditions and skylight distributions using the horizontal global daylight illuminance that is measured by the fixed sensors.

Keywords: Diffuse skylight, Building energy saving, anisotropic sky, Fourier transfer

1. Introduction

The building stocks use half of the total energy for subtropical cities [1]. The solar energy is essential to the building energy savings. The solar heat gain through building envelop leads to the cooling needs in summer [2] while compensates part of the heating demands in winter. The visible light saves the artificial lighting energy and prevents the resulted heat dissipation. The solar heating and photovoltaic techniques provide renewable energy on site [3]. The solar and daylight energy on building envelop in various directions are thus the cornerstone for active and passive building energy saving techniques.

The solar energy on building envelop are composed of the direct, diffuse and reflected parts. Studies showed that half of the solar radiation on horizontal and vertical planes was composed by the diffuse part [4]. However, the diffuse radiation and daylight data were usually estimated by models because of the high measurement costs, and the difficulties to take measurements for many different directions.

Different regions in the sky dome may have different sky radiance and brightness, and contribute to the solar energy and daylight evaluations differently. For clear skies, the forward scattering by air leads to an anisotropic sky radiance distribution that peak around the sun and weaken rapidly for the sky far away. For overcast skies, however, the cloud and mist may lead to azimuthal homogenous radiance and luminance distribution. For buildings in cities, the surrounding buildings may obstruct a part of the skydome, and weaken the diffuse skylight irregularly. In such condition, the sky radiance and luminance from unobstructed sky regions can be important for radiation and daylight on surfaces.

Previously developed skylight models differed from the early-stage uniform diffuse sky model to the later models [5, 6] that assumed anisotropic sky radiance variation discontinuously. In 1998, Kittler et al. [7] proposed a set of sky models that described continuous sky luminance variations in different sky regions for 15 different conditions from overcast to partly cloudy and clear. In 2003, the International Commission on Illumination (CIE) accepted the models as the CIE Standard Skies [8].

Many worldwide studies reported the Skies described the skylight distribution well [9], and the model was more accurate than other similar ones [10]. Since the daylight is the visible part of the solar energy, the model for skylight luminance has been used in sky radiance studies as well.
Though the models were well developed, there is no official criterion to judging the overcast, partly cloudy, and clear conditions, and selecting the CIE Sky models accordingly. Measuring sky luminance distribution [11] can be inclusive yet costly, and such data were accessible in a few places in the world. Alternative approaches identified the conditions by vertical diffuse radiation and skylight illuminance [12] suffered from data measurement problems as well. An approach [13] using horizontal sunlight measurements and its indices mixed a part of the partly cloudy skies with either clear or overcast skies. For overcast and partly cloudy skies, the randomly distributed cloud may cause the horizontal global daylight data to fluctuate in high frequency. For clear skies, in contrast, the daylight and radiation would vary smoothly by solar altitude angle. Fourier Transfer [14] is fundamental to study the data series variation frequencies. It is thus possible to identify the sky conditions via the Fourier Transfer analysis of the global illuminance on the horizontal surfaces. The approach was studied in the current work using the CIE Standard Sky by the sky luminance scan in Hong Kong in 2004. The daily time series of horizontal global illuminance were analyzed using the Fourier Transfer for the variations in high and low frequencies. Features of the daylight clearness index series in the frequency domain for overcast, partly cloudy and clear skies were reported and discussed.

2. Data measurements and pre-processing

The diffuse sky luminance of 145 sky directions was measured by sky scanner EKO MS-301LR. The scanner scrolls its luminance and radiance sensors in altitude and azimuth directions. The sensor view angle is 11 degrees, and the 145 measurements covered 68% of the skydome. Direct sunlight greater than 35 kcd/m^2 was prevented to protecting the sensor. Both the sky luminance and the horizontal global illuminance were recorded every 10 minutes at City University of Hong Kong (CityUHK) from Jan. to Dec. 2004. Our previous work described the measurements in detail.
The data quality control excluded datasets with negative luminance recordings, and the horizontal illuminance less than zero or recorded at solar altitude angle less than 4 degrees. Low illuminance data were conserved to keep its time series complete, and preventing interpolations for the missing or rejected data. In total, 21,809 sets of luminance data and 23,083 sets of horizontal global illuminance data were properly recorded. Both measurements were in a 10-minute interval.

3. Methodology

The work evaluates horizontal global daylight illuminance and its clearness index K_t of different CIE Standard Skies. K_t is the ratio of horizontal global daylight illuminance on the ground to horizontal extraterritorial illuminance. The horizontal global daylight illuminance daily series in 10 minutes interval was analyzed by the Fast Fourier Transfer (FFT) for its components that variated in high and low frequencies. The CIE models describe the luminance distributions of the five overcast, five partly cloudy and five clear skies by its well-defined equations. Comparing the sky luminance scan against the 15 CIE Standard Sky models determines the overcast, partly cloudy and clear sky conditions.

3.1. The CIE Standard Skies

The 15 CIE Sky models depict the relative luminance ($L_{\alpha\phi}$, cd/m^2) of a sky point at sky altitude α and azimuth ϕ to that at the zenith point (L_Z, cd/m^2), as given by Eq. 1. Z is the zenith angle of the sky element at α, $Z = \pi/2 - \alpha$. $\varphi(Z)/\varphi(0)$ is the relative gradation function, and $f(\chi)/f(Z_S)$ is the relative indicatrix function, given by Eqs. 2 and 3, respectively. χ is the angular distance between the sky element at (α, ϕ) and the sun, $\cos\chi = \cos Z_S \cos Z + \sin Z_S \sin Z \cos|\phi - \phi_S|$, Z_S is the solar zenith angle, and ϕ_S is the solar azimuth angle. The gradation function depicts the sky luminance variation from sky zenith to horizon. The indicatrix function marks the luminance attenuation from the sun to the sky parts that are far away. Coefficients *a* to *e* can be adjusted for different variation rates in different parts of the sky dome, which represents different sky conditions from overcast to clear.

$$\frac{L_{\alpha\phi}}{L_Z} = \frac{f(\chi)\varphi(Z)}{f(Z_S)\varphi(0)} \tag{1}$$

$$\frac{\varphi(Z)}{\varphi(0)} = \frac{1 + a\exp(b/\cos Z)}{1 + a\exp b} \tag{2}$$

$$\frac{f(\chi)}{f(Z_S)} = \frac{1 + c\left[\exp(d\chi) - \exp(d\pi/2)\right] + e\cos^2\chi}{1 + c\left[\exp(dZ_S) - \exp(d\pi/2)\right] + e\cos^2 Z_S} \tag{3}$$

3.2. Identifying the CIE Standard Skies by luminance scan

The scanner measures the sky luminance (L_i, cd/m^2, i =1 to 145) in 145 sky directions for 68% of the sky. The most straightforward approach to identifying the CIE skies is comparing the measured luminance distribution against the CIE models. However, for sites with a low latitude of 22.3 degrees, the sun would approach the sky zenith at summer solar noon, which imposes sunlight instead of the skylight to the zenith measurements. Thus, the measured luminance was normalized by the horizontal illuminance instead of the zenith luminance L_Z using the Tregenza approach [15]. The CIE sky model that gave the least root mean square error against the normalized measurements represented the luminance distribution, and points out the overcast, partly cloudy or clear sky condition.

3.3. Frequency analysis by Fast Fourier Transfer

Fast Fourier Transfer (FFT) in MATLAB toolbox was used for discrete data series [14]. The absolute value of the FFT results denotes the frequency amplitude in the time-domain. For time series with N illuminance I_j samples, the kth term of the Fourier transfer is denoted as S_k (j and k = 1 to N). Given sampling frequency F_s (144/day for 10-min interval), the frequency for k was $F_s(k-1)/N$.

It can be difficult to evaluate the Sky type and the variation feature correlations by profiles. Thus, we weighted the daylight illuminance S_k at different frequencies by w_k defined as Equation 4, and defined the frequency factor F given as Equation 5. The ratio of (k−1) to (N/2) gives the relative significance of frequency k to the highest frequency under study. Higher weights were given to S_k at high frequencies, leading to a significant F for daylight profile that variated in a high frequency. a and b are constant coefficients. b defines the high and low-frequency threshold while a gives the weight variation speed around the threshold. We set a as 20 for the current study, which depicts a fast increase of the weight from 0 to 1 at the threshold b and a "hard" cut off for the low-frequency terms.

$$\omega_k = \frac{1}{1 + \exp\left(-a\left[(k-1)/(N/2) - b\right]\right)} \tag{4}$$

$$F = \left[\sum(w_k S_k)\right] / \sum S_k \tag{5}$$

Apart from the cloud coverage, however, the high frequency could result from the noises and data series discontinuities even though the data series is smooth. A solution is removing the low amplitude terms in the frequency domain. However, it can be difficult to set a hard threshold for removing the low amplitude terms without harming the data integrity. A systematic approach will be discussed later.

4. Results and discussions

4.1. CIE Standard Skies frequency of occurrence

Figure 1 gives the occurrence frequency of the CIE Standard Skies according to the sky luminance scan in the 10-minute interval. The figure shows that 37, 40 and 23% of the data sets were overcast, partly cloudy and clear skies, respectively. It can be surprising that the partly cloudy skies took such a high frequency. The most frequent skies of overcast, partly cloudy and clear skies were Skies 1, 8 and 13. The results were similar to another local [11], and an overseas work in similar climate [9].

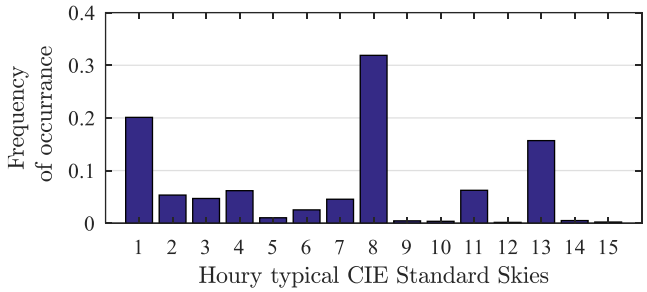

Figure 1. The occurrence frequency of CIE Standard Skies in the 10-minute interval

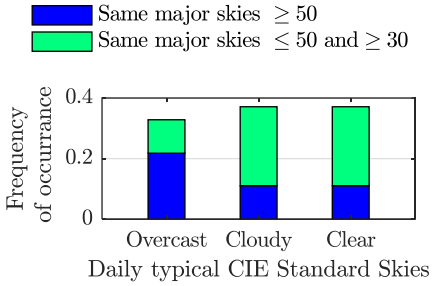

Figure 2. Occurrence frequency of daily overcast, partly cloudy and clear skies

Major sky type of the day plotted in Figure 2 was the most frequent overcast, partly cloudy or clear skies throughout the day. For the 73 measurements from 6:00 to 18:10, the major daily sky determined by more than 50, and 30 to 50 measurements in 10-minute interval were plotted separately. In total, 318 days with more than 30 consistent sky recordings in 10-miniute interval were accepted. The remaining 48 days were excluded since their 10-minute sky types were inconsistent during the day.

4.2. Daily clearness index profiles in time and frequency domains

Figure 3 (a) shows the daily horizontal global illuminance (I_{HG}) and its clearness index (K_t) profiles in the time domain for cloudy skies. The profile of I_{HG} in the frequency domain was similar to K_t. For the day dominated by the partly cloudy skies, both I_{HG} and K_t variated in high frequency throughout the measurement period. The randomly distributed clouds would block the direct sunlight recurrently, which probably lead to the irregular illuminance drops in its time series and the illuminance fluctuations in high frequency. Figure 3 (b) gives the I_{HG} components in various variation frequencies. We analyzed I_{HG} instead of K_t because I_{HG} was close to a normal distribution especially for clear skies, and there would be less high frequency terms due to the data discontinuity. Considering the sampling interval of 10 minutes and a total sample size of 36 during the daytime, the frequency of 10, for example, indicates an illuminance drop every 72 minutes. The figure quantifies I_{HG} at different variation frequencies and reveals noticeable I_{HG} components at frequencies greater than 10 times per day. The highest I_{HG} component at low frequency was due to daily solar altitude variation.

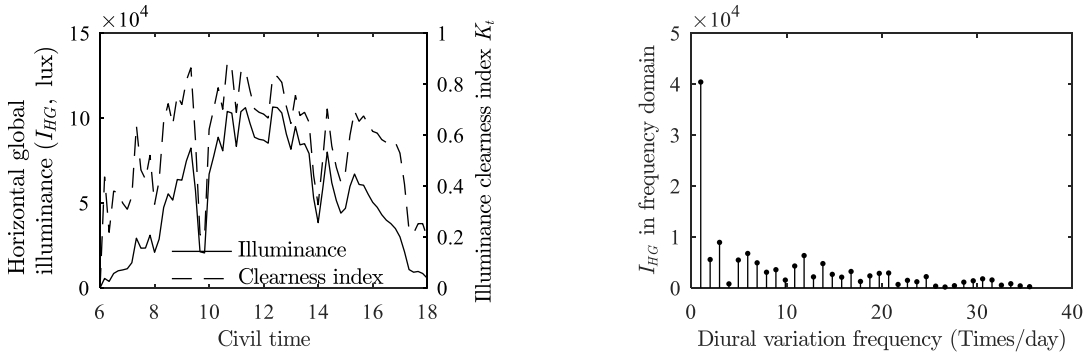

(a) (b)

Figure 3. (a) Daily horizontal global illuminance and its clearness index in the time domain for cloudy skies; (b) Horizontal global illuminance in the frequency domain for cloudy skies

Figure 4 (a) gives the typical I_{HG} and K_t variations in time and frequency domains under clear skies. For the day that is dominated by the clear skies, the illuminance variated smoothly throughout the day, and its daily profile was in a bell shape. Compared to the partly cloudy skies in Figure 3, less I_{HG} and K_t variations in time domain were found for the day of clear skies. For clear skies, the sky was free of

clouds, and the I_{HG} and K_t were affected mainly by the solar altitude that variated smoothly during the day. Figure 4 (b) quantifies I_{HG} in different frequencies. Compared to the cloudy skies, the daily I_{HG} series of clear skies rarely fluctuated in frequencies greater than 2, which corresponded to a 6-hour interval. The findings via the frequency profile indicated stable illuminance variations during the day.

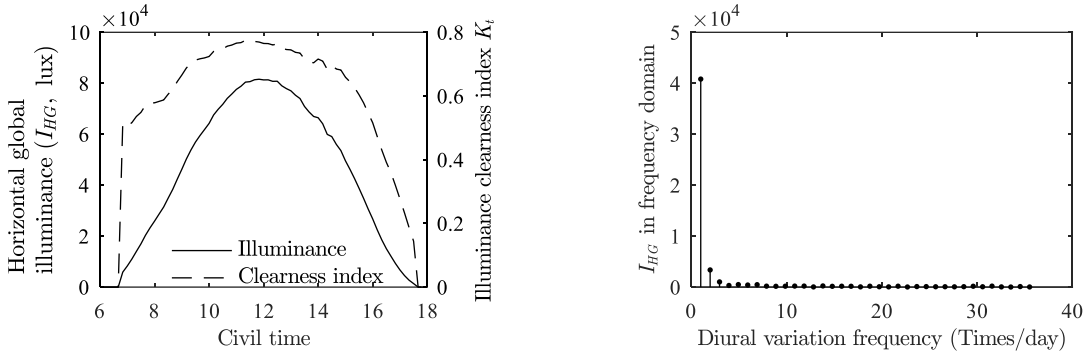

Figure 4. (a) Daily horizontal global illuminance and its clearness index in the time domain for clear skies; (b) Horizontal global illuminance in the frequency domain for clear skies

4.3. Daily clearness index and variation features for different skies

Figure 5 plots the daylight clearness index K_t and fluctuation factor F CIE overcast, partly cloudy and clear skies for the whole day. The cutting threshold b for high and low frequencies in Equation 7 was set as 0.6 by empirical trial and error tests. We removed the frequency terms that were less than two times of the 4th lowest frequency term to avoid noise impacts. The figure shows that K_t = 0.4 was a good criterion for separating the overcast and daily partly cloudy skies. K_t = 0.6 can be a potential threshold to separating the daily partly cloudy and clear skies. However, there were a few partly cloudy days whose K_t was greater than 0.6, though their daily sky conditions were supported by less than 50 sky scans per day. It is noticeable that the fluctuation feature of K_t, denoted by F, can be a supplementary criterion to identifying the clear and partly cloudy skies. Most of the clear skies were featured by an F less than 0.07 due to the stable daylight and its index K_t during the days clear of clouds. Thus, F would improve separating the partly cloudy and clear skies at high daily K_t. The overlapped partly cloudy and clear skies in the figure was probably because of the sky condition changing during the day. Selecting different thresholds b for high and low-frequency terms can lead to different F, yet its relative significance for overcast, partly cloudy and clear skies would not change.

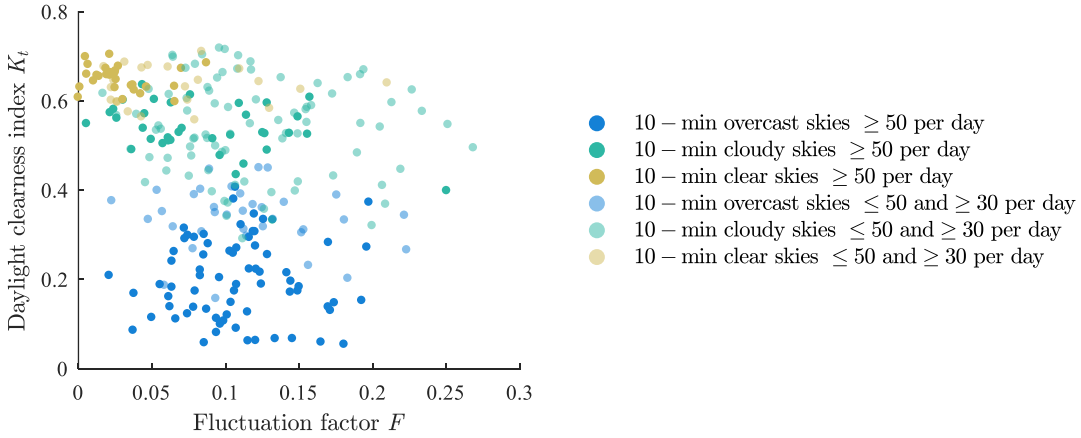

Figure 5. F and K_t of CIE overcast, partly cloudy and clear skies in the daily interval

5. Conclusions and future works

The current work attempted to identifying the daily CIE Standard overcast, partly cloudy and clear skies using the horizontal global illuminance data only. We analyzed the daily series of the horizontal global illuminance by transferring it from the time domain to the frequency domain. The daily global horizontal illuminance I_{HG} series of clear skies was featured by the low amplitude terms in high frequency, owing to the stable sunlight from the sky clear of clouds. The overcast and partly cloudy skies, in comparison, were featured by high-frequency terms greater than the clear skies, probably due to the frequent sunlight coverage by clouds. The frequency domain profiles were summarized by assigning greater weights to the high-frequency terms for a weighted total, which was defined as the fluctuation factor. For I_{HG} in the frequency domain, we assigned weight close to 1 for those whose frequency was greater than 60% of the maximum, and setting 0 for the rest. Finally, we found greater fluctuation factors for overcast and partly cloudy skies compared to the relative lower fluctuation factor for clear skies. The fluctuation factors for most clear skies were less than 0.075 by the current weight settings, which can improve identifying the partly cloudy and clear skies whose daily K_t was greater than 0.6.

A limitation of the current work is that the data series were in the daily interval. However, the data series for an hour or half day may not begin and end at zero. Such discontinuity at the series head and tails can lead to many low-amplitude, high-frequency terms even though the data series is smooth in the time domain. A systematic approach to solve this problem will be presented in future work.

Acknowledgments

The work was under the project *A Fundamental Study of Anisotropic Sky Radiance and its Effect on Building Envelopes in City Environments* supported by National Natural Science Foundation of China (ID: 51808139).

References

[1] EMSD 2017 *Hong Kong Energy End-use Data* (Hong Kong: Electrical & Mechanical Services Dept.)
[2] Lam J C 2000 Energy analysis of commercial buildings in subtropical climates *Building and Environment* vol 35 pp 19-26
[3] Li D H W, Chow S K H and Lee E W M 2013 An analysis of a medium size grid-connected building integrated photovoltaic (BIPV) system using measured data *Energy and Buildings* vol 60 pp 383-387
[4] Liang H, Li S K, Ma J Y and Luo Y 2011 Variation trend of direct and diffuse radiation in China over recent 50 years *Acta Physica Sinica* vol 60(6) pp 069601
[5] Klucher T M 1979 Evaluation of models to predict insolation on tilted surfaces *Solar Energy* vol 23 pp 111-114
[6] Perez R, Ineichen P, Seals R, Michalsky J and Stewart R 1990 Modeling daylight availability and irradiance components from direct and global irradiance *Solar Energy* vol 44 pp 271-289
[7] Kittler R, Darula S and Pereze R 1998 *A set of standard skies* (Bratislava: Polygrafia SAC)
[8] CIE 2003 *Spatial Distribution of Daylight - CIE Standard General Sky* (Vienna: CIE Central Bureau)
[9] Wittkopf S K and Soon L K 2007 Analysing sky luminance scans and predicting frequent sky patterns in Singapore *Lighting Research & Technology* vol 39 pp 31-51
[10] Yun S I and Kim K S 2018 Sky Luminance Measurements Using CCD Camera and Comparisons with Calculation Models for Predicting Indoor Illuminance *Sustainability* vol 10(5) pp 1556
[11] Ng E, Cheng V, Gadi A, Mu J, Lee M and Gadi A 2007 Defining standard skies for Hong Kong *Building and Environment* vol 42 pp 866-876
[12] Li D H W, Chau T C and Wan K K W 2014 A review of the CIE general sky classification approaches *Renewable and Sustainable Energy Reviews* vol 31 pp 563-74
[13] Lou S, Li D H W and Lam J C 2017 CIE Standard Sky classification by accessible climatic indices. *Renewable Energy* vol 113 pp 347-56

[14] Frigo M and Johnson S G 1998 FFTW: an adaptive software architecture for the FFT *Proceedings of the International Conference on Acoustics, Speech and Signal Processing* vol 3 pp 1381-1384
[15] Tregenza P R 2004 Analysing sky luminance scans to obtain frequency distributions of CIE Standard General Skies *Lighting Research and Technology* vol 36 pp 271-9